

neonSoilFlux: An R Package for Continuous Sensor-Based Estimation of Soil CO₂ Fluxes

John Zobitz¹ Edward Ayres² Zoey Werbin³ Ridwan Abdi¹

⁴ Natalie Ashburner-Wright⁵ Lillian Brown⁵

⁵ Ryan Frink-Sobierajski⁵ Lajntxiag Lee¹ Dijonë Mehmeti¹

⁶ Christina Tran⁵ Ly Xiong¹ Naupaka Zimmerman^{4,5}

⁷ ¹ Augsburg University, 2211 Riverside Avenue, Minneapolis, MN 55454

⁸ ² National Ecological Observatory Network, Battelle, 1685 38th Street, Suite 100, Boulder,
⁹ CO 80301

¹⁰ ³ Boston University, 5 Cummington Street, Boston, MA 02215

¹¹ ⁴ University of Kansas, 1450 Jayhawk Boulevard, Lawrence, KS 66045

¹² ⁵ University of San Francisco, 2130 Fulton Street, San Francisco, CA 94117

13 Acknowledgments

¹⁴ John Zobitz acknowledges Kathleen O'Rourke for code development. Naupaka Zimmerman
¹⁵ thanks technical staff at USF for support with field gear assembly and shipping. We thank the
¹⁶ NEON field staff and assignable assets teams for facilitating each of the six NEON site visits.

¹⁷ We are grateful to LI-COR technical staff for helpful discussions about optimal soil chamber
¹⁸ sampling methods. This work was supported by NSF DEB grant #2017829 awarded to John
¹⁹ Zobitz, and NSF DEB grant #2017860 awarded to Naupaka Zimmerman. This material is
²⁰ based in part upon work supported by the National Ecological Observatory Network (NEON),
²¹ a program sponsored by the U.S. National Science Foundation (NSF) and operated under
²² cooperative agreement by Battelle. We also thank the reviewers and subject editor for their
²³ constructive feedback.

²⁴ **Conflict of Interest Statements**

²⁵ None of the authors have a financial, personal, or professional conflict of interest related to
²⁶ this work.

²⁷ **Author Contributions**

²⁸ Conceptualization: John Zobitz, Naupaka Zimmerman; Methodology: Edward Ayres, John
²⁹ Zobitz, Naupaka Zimmerman; Software: John Zobitz, Naupaka Zimmerman, Zoey Werbin,
³⁰ Edward Ayres, Dijonë Mehmeti, Ridwan Abdi, Ly Xiong, Lajntxiag Lee; Validation: John
³¹ Zobitz, Naupaka Zimmerman; Formal Analysis: John Zobitz, Naupaka Zimmerman, Dijonë
³² Mehmeti, Ridwan Abdi, Ly Xiong, Lajntxiag Lee; Investigation: John Zobitz, Naupaka Zimmerman,
³³ Ryan Frink-Sobierajski, Christina Tran, Natalie Ashburner-Wright, Lillian Brown;
³⁴ Resources: John Zobitz, Naupaka Zimmerman; Data curation: John Zobitz, Naupaka Zimmerman,
³⁵ Dijonë Mehmeti, Ly Xiong; Writing – original draft: John Zobitz, Naupaka Zimmerman;
³⁶ Writing – review and editing: John Zobitz, Naupaka Zimmerman, Zoey Werbin, Edward Ayres,
³⁷ Christina Tran, Dijonë Mehmeti, Ly Xiong; Visualization: John Zobitz, Naupaka Zimmerman,

³⁸ Dijonë Mehmeti, Ridwan Abdi, Ly Xiong; Supervision: John Zobitz, Naupaka Zimmerman;
³⁹ Project Administration: John Zobitz, Naupaka Zimmerman; Funding Acquisition: John Zob-
⁴⁰ itz, Naupaka Zimmerman.

⁴¹ **Data Availability**

⁴² Data available via <https://doi.org/10.5281/zenodo.17516319> (Zobitz & Zimmerman, 2025).
⁴³ Field-collected data, `neonSoilFlux` calculated outputs, and manuscript-generating code are
⁴⁴ provided within this repository.

45 **1 Abstract**

- 46 1. Accurate quantification of soil carbon fluxes is essential to reduce uncertainty in esti-
47 mates of the terrestrial carbon sink. However, these fluxes vary over time and across
48 ecosystem types and so it can be difficult to estimate them accurately across large scales.
49 The flux gradient method estimates soil carbon fluxes using co-located measurements of
50 soil CO₂ concentration, soil temperature, soil moisture, and other soil properties. The
51 National Ecological Observatory Network (NEON) provides such data across 20 ecocli-
52 climatic domains spanning the continental U.S., Puerto Rico, Alaska, and Hawai‘i.
- 53 2. We present an R software package (`neonSoilFlux`) that acquires soil environmental data
54 to compute half-hourly soil carbon fluxes for each soil replicate plot at a given terrestrial
55 NEON site. To assess the computed fluxes, we visited six focal NEON sites and measured
56 soil carbon fluxes using a closed-dynamic chamber approach.
- 57 3. Outputs from the `neonSoilFlux` showed agreement with measured fluxes (R^2 between
58 measured and `neonSoilFlux` outputs ranging from 0.04 to 0.81 depending on calculation
59 method used); measured outputs generally fell within the range of calculated uncertain-
60 ties from the gradient method. Calculated fluxes from `neonSoilFlux` aggregated to the
61 daily scale exhibited expected site-specific seasonal patterns.
- 62 4. While the flux gradient method is broadly effective, its accuracy is highly sensitive to
63 site-specific inputs, including the extent to which gap-filling techniques are used to in-
64 terpolate missing sensor data and to estimates of soil diffusivity and moisture content.
65 Future refinement and validation of `neonSoilFlux` outputs can contribute to existing
66 databases of soil carbon flux measurements, providing near real-time estimates of a crit-
67 ical component of the terrestrial carbon cycle.

68 **1.1 Keywords**

69 Soil carbon, carbon dioxide, flux gradient, carbon cycle, field validation, soil respiration, ecosys-
70 tem variability, diffusion

71 **2 Introduction**

72 Soils contain the planet's largest reservoir of terrestrial carbon (Jobbág & Jackson, 2000). A
73 critical component of this reservoir is soil organic matter, the accumulation of which is influ-
74 enced by biotic factors such as above-ground plant inputs (Jackson et al., 2017). These inputs
75 in turn are influenced by environmental factors such as growing season length, temperature,
76 and moisture (Desai et al., 2022), which also affect the breakdown of soil organic matter and its
77 return to the atmosphere. Across heterogeneous terrestrial landscapes, the interplay between
78 these biotic and abiotic factors influence the size of the soil contribution to the terrestrial
79 carbon sink (Friedlingstein et al., 2025). However, the heterogeneity of these processes across
80 diverse ecosystems in the context of rapid environmental change leads to large uncertainty
81 about the magnitude of this sink in the future, and thus there remains a pressing need to
82 quantify changes in soil carbon pools and fluxes across scales.

83 Ecological observation networks such as the United States' National Ecological Observatory
84 Network (NEON) and others (e.g. the globally-distributed FLUXNET or the European Inte-
85 grated Carbon Observation System) present a significant advancement in the nearly continuous
86 observation of biogeochemical processes at the continental scale. Notably, at 47 terrestrial sites
87 across the continental United States that span 20 ecoclimatic domains, NEON provides half-
88 hourly measurements of soil CO₂ concentration, temperature, and moisture at different vertical
89 depths. Each of these NEON sites also encompasses measurements of the cumulative sum of all
90 ecosystem carbon fluxes in an airshed using the eddy covariance technique (Balocchi, 2014).

91 Soil observations provided by NEON are on the same timescale and standardized with eddy co-
92 variance measurements from FLUXNET. These types of nearly continuous observational data
93 (NEON and FLUXNET) can be used to reconcile differences between model-derived or data-
94 estimated components of ecosystem carbon flux (Jian et al., 2022; Luo et al., 2011; Phillips et
95 al., 2017; J. Shao et al., 2015; P. Shao et al., 2013; Sihl et al., 2016).

96 Estimated or observed soil carbon fluxes are a key metric for understanding change in soil
97 carbon pools over time (Bond-Lamberty et al., 2024). A soil carbon flux to the atmosphere
98 (F_S , units $\mu\text{mol m}^{-2} \text{ s}^{-1}$), represents the aggregate process of transfer of soil CO_2 to the
99 atmosphere from physical and biological processes (e.g. diffusion and respiration). Soil carbon
100 fluxes can be assumed to encompass soil carbon respiration from autotrophic or heterotrophic
101 sources (Davidson et al., 2006) and modeled with a exponential Q_{10} paradigm (Bond-Lamberty
102 et al., 2004; Chen & Tian, 2005; Hamdi et al., 2013).

103 One common method by which F_S is measured in the field is through the use of soil chambers
104 in a closed, well-mixed system (Norman et al., 1997) with headspace trace gas concentrations
105 measured with an infrared gas analyzer (IRGA). F_S can also be estimated from soil CO_2
106 measurements at different depths in the soil using the flux-gradient method (Maier & Schack-
107 Kirchner, 2014). Closed-chamber IRGA measurements, while being the most common method,
108 require either frequent in-person site visits or expensive and fragile automated systems. The
109 potential of the gradient method is that fluxes can be estimated from continuous data recorded
110 by robust solid-state sensors. The flux-gradient method is an approach that uses conservation
111 of mass to calculate flux at a vertical soil depth z at steady state by applying Fick's law of
112 diffusion. A simplifying assumption for the flux-gradient method is that there is no mass trans-
113 fer in the other spatial dimensions x and y (Maier & Schack-Kirchner, 2014). The diffusivity
114 profile, a key component of this calculation, varies across the soil depth as a function of soil
115 temperature, soil volumetric water content, atmospheric air pressure, and soil bulk density

116 (Millington & Shearer, 1971; Moldrup et al., 1999; Sallam et al., 1984).

117 Databases such as the Soil Respiration Database (SRDB) or the Continuous Soil Respiration
118 Database (COSORE) add to the growing network of resources for making collected observa-
119 tions of soil fluxes available to other researchers (Bond-Lamberty, 2018; Bond-Lamberty et
120 al., 2020; Bond-Lamberty & Thomson, 2010; Jian et al., 2021; Jiang et al., 2024). However,
121 these databases currently encompass primarily direct soil measurements of fluxes (i.e. those
122 using methods like the closed-chamber method described above). Currently, NEON provides
123 all measurements to calculate F_S from Fick's law, but soil flux as a derived data product was
124 descoped from the initial network launch due to budget constraints (Berenbaum et al., 2015).
125 Deriving estimates of F_S using continuous sensor data across NEON sites using NEON data
126 thus remains a high priority.

127 This study describes an R software package, `neonSoilFlux`, that computes a standardized
128 estimate of F_S at all terrestrial NEON sites using the flux-gradient method. Using direct
129 chamber-based field observations of soil carbon dioxide flux from a subset of terrestrial NEON
130 sites spanning six states, we provide a direct validation of F_S from `neonSoilFlux`. While
131 open source R software tools currently exist for processing chamber-based flux measurements
132 (Jurasinski et al., 2022; Pedersen, 2024; Rheault et al., 2024; Wilson et al., 2024; Zhao, 2019),
133 to our knowledge this is the first package that incorporates NEON data directly.

134 Key objectives of this study are to:

- 135 1. Apply the flux-gradient method to estimate soil CO₂ flux from continuous sensor mea-
136 surements across six NEON sites.
- 137 2. Benchmark estimated soil carbon fluxes against field measurements (e.g. direct chamber
138 measurements of soil flux).

- 139 3. Identify sources of error in the flux-gradient approach across diverse sites in order to
140 guide future work.

141 **3 Materials and Methods**

142 **3.1 Field methods**

143 **3.1.1 Focal NEON Sites**

144 In order to acquire field data to validate model predictions of flux, we selected six terrestrial
145 NEON sites for analysis. We conducted roughly week-long field measurement campaigns at
146 these sites, which span a range of environmental gradients and terrestrial domains (Table 1).
147 SJER, SRER, and WREF were visited during May and June of 2022, and WOOD, KONZ,
148 and UNDE during May and June of 2024.

149 **3.1.2 Soil collar placement**

150 Either one (2022 sampling campaign) or two (2024 sampling campaign) PVC soil collars (20.1
151 cm inside diameter) were installed in close proximity to the permanent NEON soil sensors at
152 each site (Figure 1). As instruments in the NEON soil sensor arrays can occasionally break
153 down or stop working, the specific soil plot where we made measurements was chosen at each
154 site in consultation with NEON staff to maximize likelihood of quality soil sensor measurements
155 during the duration of the IRGA measurements. The plot selected at each site (out of the 5 in
156 each replicate array at each site) are presented in the last column of Table 1. After installation,
157 collar(s) were left to equilibrate for approximately 24 hours prior to any measurements being
158 taken.

159 **3.1.3 Infrared gas analyzer measurements of soil CO₂ flux**

160 In 2022, we then made measurements of flux on an hourly interval for 8 hours each day.
161 Measurements were taken from roughly 8 am to 4 pm, with the time interval selected to
162 capture the majority of the diurnal gradient of soil temperature each day. These measurements
163 were made using a LI-6800 infrared gas analyzer instrument (LI-COR Environmental, Lincoln,
164 NE) fitted with a soil chamber attachment (attachment 6800-09). In 2024, we again used the
165 same LI-6800 instrument, but made half-hourly measurements over an approximately 8 hour
166 period. In addition, in 2024 we also installed a second collar and used a second instrument, an
167 LI-870 CO₂ IRGA, connected to an automated robotic chamber (LI-COR chamber 8200-104)
168 controlled by an LI-8250 multiplexer to make automated measurements. The multiplexer was
169 configured to take half-hourly measurements 24 hours a day for the duration of our sampling
170 bout at each site. Each instrument was paired with a soil temperature and moisture probe
171 (Stevens HydraProbe, Stevens Water, Portland, OR) that was used to make soil temperature
172 and moisture measurements concurrent with the CO₂ flux measurements. Chamber volumes
173 were set by measuring collar offsets at each site. System checks were conducted daily for the
174 LI-6800 and weekly for the LI-8250. Instruments were factory calibrated before each field
175 season.

Table 1: Listing of NEON sites studied for field work and analysis. Site refers to NEON site codes: Santa Rita Experimental Range (SRER), San Joaquin Experimental Range (SJER), Wind River Experimental Forest (WREF), Chase Lake National Wildlife Refuge (WOOD), Konza Prairie Biological Station (KONZ), and the University of Notre Dame Environmental Research Center (UNDE). Location is reported in decimal degrees of latitude and longitude. Other abbreviations include Mean Annual Temperature (MAT); \bar{T}_S : average soil temperature during field measurements; \bar{SWC} : average soil water content during field measurements. Dates refer to field measurement dates for each site. Plot refers to the particular location in the soil sensor array (denoted as HOR by NEON) where field measurements were made.

Site	Location	Ecosystem	MAT	\bar{T}_S	MAP	\bar{SWC}	Dates	Plot
SRER	31.91068, -110.83549	Shrubland	19.3 °C	47.6 °C	346 mm	4.0%	May 29– June 1 2022	004

Table 1: Listing of NEON sites studied for field work and analysis. Site refers to NEON site codes: Santa Rita Experimental Range (SRER), San Joaquin Experimental Range (SJER), Wind River Experimental Forest (WREF), Chase Lake National Wildlife Refuge (WOOD), Konza Prairie Biological Station (KONZ), and the University of Notre Dame Environmental Research Center (UNDE). Location is reported in decimal degrees of latitude and longitude. Other abbreviations include Mean Annual Temperature (MAT); \bar{T}_S : average soil temperature during field measurements; \bar{SWC} : average soil water content during field measurements. Dates refer to field measurement dates for each site. Plot refers to the particular location in the soil sensor array (denoted as HOR by NEON) where field measurements were made.

Site	Location	Ecosystem	MAT	\bar{T}_S	MAP	\bar{SWC}	Dates	Plot
SJER	37.10878, -119.73228	Oak woodland	16.4 °C	41.7 °C	540 mm	1.2%	June 1–4 2022	005
WREF	45.82049, -121.95191	Evergreen forest	9.2 °C	15.3 °C	2225 mm	27.2%	June 7–9 2022	001
WOOD	47.1282, -99.241334	Restored prairie	4.9 °C	14.9 °C	495 mm	14.9%	June 3–9 2024	001
KONZ	39.100774, -96.563075	Tallgrass prairie	12.4 °C	23.4 °C	870 mm	23.4%	May 29– June 1 2024	001
UNDE	46.23391, -89.537254	Deciduous forest	4.3 °C	13.0 °C	802 mm	13.0%	May 22–25 2024	004

176 3.1.4 Post-collection processing of field data

177 We used LI-COR SoilFluxPro software (v 5.3.1) to assess the data after collection and to inform
 178 sampling parameters. We checked appropriateness of dead band and measurement durations
 179 using built-in evaluation tools. Based on this, the deadband period was set for 30-40 seconds,
 180 depending on the site, and the measurement duration was 180 seconds with a 30 second pre-
 181 purge and a 30 second post-purge at most sites, and a 90 second pre- and post-purge at sites
 182 with higher humidity due to recent precipitation events. We also assessed the R^2 of linear and
 183 exponential model fits to measured CO₂ to verify measurement quality.

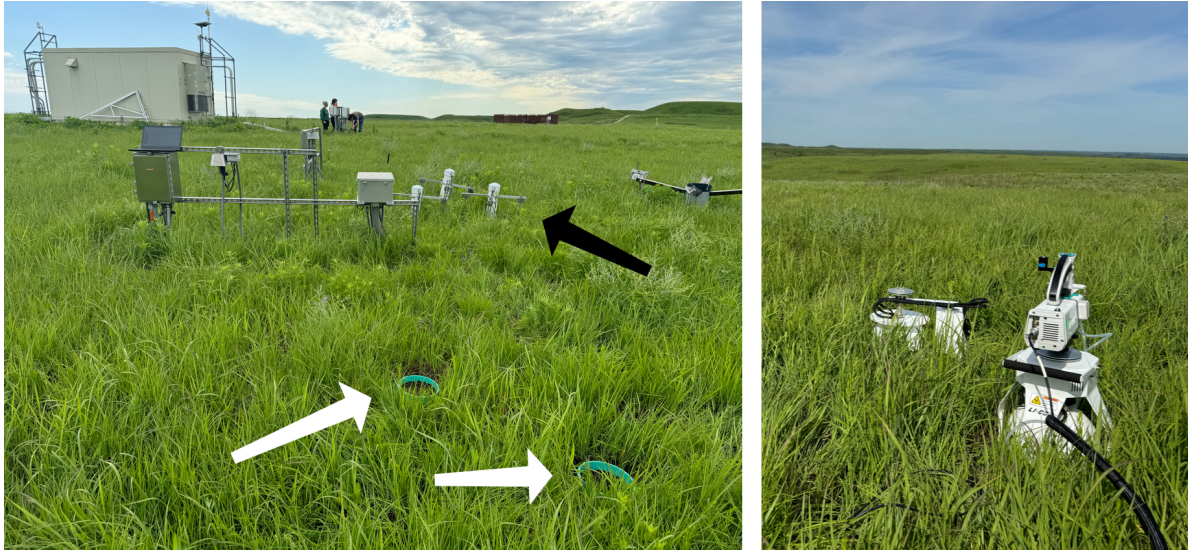


Figure 1: Spatial layout of field sampling using a closed-dynamic chamber setup at a representative NEON site (KONZ). Left image shows collars (white arrows) and permanent soil sensor installation (black arrow) and right image shows the LI-6800 (foreground) and LI-8200-104 (background) instruments placed on the collars.

¹⁸⁴ **3.2 neonSoilFlux R package**

¹⁸⁵ We developed an R package called `neonSoilFlux` (Zobitz et al., 2024) to compute half-hourly
¹⁸⁶ soil carbon fluxes and uncertainties from NEON data. The objective of the `neonSoilFlux`
¹⁸⁷ package is a unified workflow (Figure 2) for soil data acquisition and analysis that supplements
¹⁸⁸ the existing `neonUtilities` data acquisition R package (Lunch et al., 2025).

¹⁸⁹ At a given NEON site there are five replicate soil plots, each with measurements of soil
¹⁹⁰ CO₂ concentration, soil temperature, and soil moisture at different depths (Figure 3). The
¹⁹¹ `neonSoilFlux` package acquires measured soil CO₂ concentration (NEON, 2024b), soil tem-
¹⁹² perature (NEON, 2024d), soil water content (NEON, 2024e), barometric pressure from the
¹⁹³ nearby tower (NEON, 2024a), and soil properties (e.g. bulk density) (NEON, 2024c) from a
¹⁹⁴ range of different NEON data products. The static soil properties were collected by NEON
¹⁹⁵ staff from a nearby soil pit during initial site characterization and are assumed to be constant

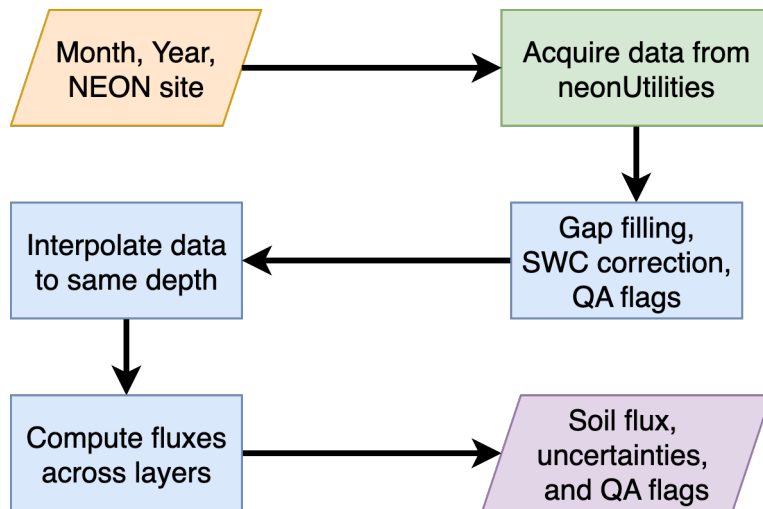


Figure 2: Diagram of `neonSoilFlux` R package. For a given month, year, and NEON site (orange parallelogram), the package acquires all relevant data to compute F_S using the `neonUtilities` R package (green rectangle). Data are gap-filled according to reported QA flags and adjusted for changes in soil water content (SWC) calibration coefficients, then interpolated to the same measurement depth before computing the soil flux, uncertainties, and final QA flags (blue rectangles). The package reports the associated soil flux, uncertainties, and quality assurance (QA) flags for the user (purple parallelogram).

196 at each site. A soil flux calculation is computed at each replicate soil plot.

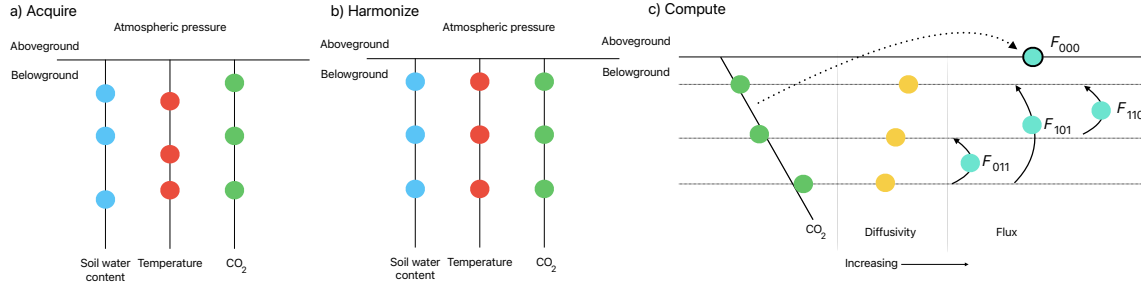


Figure 3: Model diagram of the data workflow for the `neonSoilFlux` R package. a) Acquire: Data are obtained for a given NEON location and horizontal sensor location, which includes soil water content, soil temperature, CO₂ concentration, and atmospheric pressure. All data are screened for quality assurance; if gap-filling of missing data occurs, it is flagged for the user. b) Harmonize: Any belowground data are then harmonized to the same depth as CO₂ concentrations using linear regression. c) Compute: The flux across a given depth is computed via Fick's law, denoted with F_{ijk} , where i , j , or k are either 0 or 1 denoting the layers the flux is computed across ($i = \text{closest to surface}$, $k = \text{deepest}$). F_{000} represents a flux estimate where the gradient dC/dz is the slope of a linear regression of CO₂ with depth.

197 The workflow to compute a value of F_S with `neonSoilFlux` consists of three primary steps,
 198 illustrated in Figure 3. First, NEON data are acquired for a given site and month via the
 199 `neonUtilities` R package (yellow parallelogram and green rectangle in Figure 2 and Panel a
 200 in Figure 3). Acquired environmental data can be exported to a comma separated value file for
 201 additional analysis. Quality assurance (QA) flags are reported as an indicator variable. Since
 202 the calibration coefficients on the soil water content sensors have changed over time (NEON,
 203 2024e), raw sensor measurements were back-calculated and soil-specific calibrations were ap-
 204 plied following Ayres et al. (2024) to generate a consistent time series at each measurement
 205 location.

206 The second step is harmonizing the data to compute soil fluxes across soil layers. This step
 207 consists of three different actions (blue rectangles in Figure 2 and Panel b in Figure 3). If a
 208 given observation by NEON is reported as not passing a quality assurance check, we applied

209 a gap filling method to replace that measurement with its monthly mean at that same depth
210 (Section 3.2.1). Belowground measurements of soil water and soil temperature are then inter-
211 polated to the same depth as soil CO₂ measurements. The diffusivity (Section 3.2.2) and soil
212 flux across different soil layers (Section 3.2.3) are then computed.

213 The third and final step is computing a surface soil flux through extrapolation to the sur-
214 face (purple parallelogram in Figure 2 and Panel c in Figure 3). Uncertainty on a soil flux
215 measurement is computed through quadrature. An aggregate quality assurance (QA) flag
216 for each environmental measurement is also reported, representing if any gap-filled measure-
217 ments were used in the computation of a soil flux. Within the soil flux-gradient method,
218 several different approaches can be used to derive a surface flux (Maier & Schack-Kirchner,
219 2014); the `neonSoilFlux` package reports four different possible values for soil surface flux
220 (Section 3.2.3) for each of two different methods of diffusivity estimation, for a total of eight
221 estimates of flux.

222 3.2.1 Gap-filling routine

223 NEON reports QA flags as binary values for each measurement and half-hourly interval. For
224 a given half-hour, if any input variable (soil CO₂ concentration, soil temperature, or soil
225 moisture) at depth z is flagged, computation of F_S is not possible. To address this, flagged
226 measurements and their uncertainties were replaced with a bootstrapped monthly mean (\bar{m})
227 and monthly standard deviation (\bar{s}) (Efron & Tibshirani, 1994).

228 For each month, depth z , and variable, we computed bootstrapped estimates of \bar{m} and \bar{s}
229 from the vectors of unflagged measurements (**m**), reported standard errors (σ), and the 95%
230 confidence interval (ϵ , or expanded uncertainty; Farrance & Frenkel (2012)). We also defined

231 a bias vector $\mathbf{b} = \sqrt{\epsilon^2 - \sigma^2}$, which quantifies the spread of uncertainty in a given period and
232 is incorporated into \bar{m} .

233 From these, 5000 bootstrap samples were generated for \mathbf{m}, σ , and \mathbf{b} . For each sample
234 (m_k, b_k, σ_k), we generated a vector \mathbf{n} (length $N = 5000$) by drawing from a normal dis-
235 tribution with mean $m_k + b_k$ and standard deviation σ_k . The sample mean and standard
236 deviation were then computed from \mathbf{n} . The resulting distributions of sample means and
237 sample standard deviations provided the bootstrapped monthly mean (\bar{m}) and standard error
238 (\bar{s}) respectively.

239 This gap-filling procedure provides a consistent treatment across all data streams. However,
240 alternative approaches may be better suited for longer gaps (e.g., correlations with other
241 NEON measurement levels or soil plots) or for variable-specific conditions. We discuss the
242 effect of gap-filling on our results in Section 5.1.

243 3.2.2 Soil diffusivity

244 Soil diffusivity D_a at a given measurement depth is the product of the diffusivity in free air
245 $D_{a,0}$ ($\text{m}^2 \text{ s}^{-1}$) and the tortuosity ξ (no units) (Millington & Shearer, 1971).

246 We compute $D_{a,0}$ with Equation 1:

$$D_{a,0} = 0.0000147 \cdot \left(\frac{T_i + 273.15}{293.15} \right)^{1.75} \cdot \left(\frac{P}{101.3} \right) \quad (1)$$

247 where T_i is soil temperature ($^\circ\text{C}$) at depth i (NEON, 2024d) and P surface barometric pressure
248 (kPa) (NEON, 2024a).

249 Previous studies by Sallam et al. (1984) and Tang et al. (2003) demonstrated the sensitivity
250 of modeled F_S depending on the tortuosity model (ξ) used to compute diffusivity. At low
251 soil water content, the choice of tortuosity model can lead to order-of-magnitude differences
252 in D_a , which in turn affect modeled F_S . The `neonSoilFlux` package currently includes two
253 approaches to calculate ξ , representing the range of tortuosity behavior reported in Sallam et
254 al. (1984).

255 The first approach is the Millington-Quirk model (Millington & Shearer, 1971), in which
256 tortuosity depends on both porosity and soil water content:

$$\xi = \frac{(\phi - SWC_i)^{10/3}}{\phi^2} \quad (2)$$

257 In Equation 2, SWC is the soil water content at depth i (NEON, 2024e) and ϕ is the porosity,
258 which in turn is a function of soil physical properties (NEON, 2024c):

$$\phi = \left(1 - \frac{\rho_s}{\rho_m}\right) (1 - f_V) \quad (3)$$

259 In Equation 3, ρ_m is the particle density of mineral soil (2.65 g cm^{-3}), ρ_s the soil bulk density (g
260 cm^{-3}) excluding coarse fragments greater than 2 mm (NEON, 2024c), and f_V is a site-specific
261 value that accounts for the proportion of soil fragments between 2-20 mm. Soil fragments
262 greater than 20 mm were not estimated due to limitations in the amount of soil that can be
263 analyzed (NEON, 2024c). We assume that rock fragments contain no internal pores.

264 The Millington-Quirk model assumes ξ is modulated by the amount of fluid saturation in
265 soil pores (Millington & Shearer, 1971). In contrast, the Marshall model (Marshall, 1959)
266 expresses tortuosity as only a function of porosity ($\xi = \phi^{1.5}$), with ϕ defined from Equation
267 3. The Marshall model is independent of soil water content and assumes tortuosity is only

268 governed by soil structure. The `neonSoilFlux` package allows users to choose the tortuosity
269 model most appropriate for site-specific conditions and research goals.

270 **3.2.3 Soil flux computation**

271 We applied Fick's law (Equation 4) to compute the soil flux F_{ij} ($\mu\text{mol m}^{-2} \text{s}^{-1}$) across two
272 soil depths i and j :

$$F_{ij} = -D_a \frac{dC}{dz} \quad (4)$$

273 where D_a is the diffusivity ($\text{m}^2 \text{s}^{-1}$) and $\frac{dC}{dz}$ is the gradient of CO_2 molar concentration
274 ($\mu\text{mol m}^{-3}$, so the gradient has units of $\mu\text{mol m}^{-3} \text{m}^{-1}$). The soil surface flux is theoretically
275 defined by applying Equation 4 to measurements collected at the soil surface and directly
276 below the surface. Measurements of soil temperature, soil water content, and soil CO_2 molar
277 concentration across the soil profile allow for application of Equation 4 across different soil
278 depths. Each site had three measurement layers, so we denote the flux as a three-digit subscript
279 F_{ijk} with indicator variables i , j , and k indicate if a given layer was used (written in order of
280 increasing depth), according to the following:

- 281 • F_{000} is a surface flux estimate using the intercept of the linear regression of D_a with
282 depth and the slope from the linear regression of CO_2 with depth (which represents $\frac{dC}{dz}$
283 in Fick's Law). Tang et al. (2003) used this approach to compute fluxes in an oak-grass
284 savannah.
- 285 • F_{110} is a flux estimate across the two shallowest measurement layers.
- 286 • F_{011} is a flux estimate across the two deepest measurement layers.
- 287 • F_{101} is a flux estimate across the shallowest and deepest measurement layers.

288 For F_{110} , F_{011} , and F_{101} , the diffusivity used in Fick's Law is always at the deeper measurement
289 layer. When used as a surface flux estimate we assume CO₂ remains constant above this flux
290 depth. Uncertainty in all F_{ijk} values was quantified using quadrature (Taylor, 2022). These
291 computed fluxes could provide the basis for additional soil flux estimates. For example, Tang et
292 al. (2005) estimated surface flux by linearly extrapolating F_{110} and F_{011} to the soil surface.

293 **3.3 Post processing evaluation**

294 Following collection of field measurements and calculation of the soil fluxes from `neonSoilFlux`
295 package, we compared measured F_S based on closed-dynamic chamber measurements with the
296 LI-COR instruments to a given soil flux calculation from `neonSoilFlux` for each site and flux
297 computation method and quantified the relationship statistically (R^2). Finally, for a half-
298 hourly interval we also computed a *post hoc* diffusivity (D_a) using the LI-COR flux along
299 with the CO₂ surface gradient reported by NEON using the measurement levels closest to the
300 surface.

301 **4 Results**

302 **4.1 Concordance between modelled and measured soil CO₂ flux**

303 The sites we visited ranged substantially in both their annual average temperature and precip-
304 itation as well as their biome type (Table 2). These differences also influenced the wide range
305 of observed flux rates across sites.

306 The timeseries of the measured fluxes from the LI-COR 6800 and 870/8250 were compared
307 to modeled soil fluxes from the `neonSoilFlux` R package (Figure 4). We also assessed year-
308 long estimated flux time series and compared those to field measurements made at each site

Table 2: Summary of measured soil characteristics and flux results from field measurements across six NEON sites using a LI-COR 6800 (LI-870/8250 measurements omitted to enable direct comparability) via the closed-dynamic chamber method. Numeric values for soil CO₂ flux, soil temperature, and volumetric soil water content (VSWC) are the mean and standard deviation of field measurements at each site.

Site	Flux μmol m ⁻² s ⁻¹	Soil temp °C	VSWC cm ³ cm ⁻³	n
UNDE	2.55 ± 0.26	14.33 ± 0.77	0.33 ± 0.02	61
WOOD	3.02 ± 0.4	16.01 ± 1.54	0.28 ± 0.01	53
WREF	3.62 ± 0.3	15.34 ± 1.76	0.27 ± 0.06	21
KONZ	6.35 ± 0.97	27.28 ± 4.14	0.37 ± 0.01	44
SJER	0.94 ± 0.02	41.68 ± 11.22	0.01 ± 0.01	32
SRER	0.72 ± 0.09	47.64 ± 7.46	0.04 ± 0.01	32

(Figure 5). Results are reported in local time. Where applicable, sites are displayed from left to right by increasing soil temperature (Table 1). Positive values of the flux indicate that there is a flux moving towards the surface. Overall, with the exception of SRER (discussed later) the computed fluxes determined using a variety of plausible methods spanned the field-measured fluxes, but the specific flux-gradient method that best approximated field measurements varied by site.

We calculated a statistical relationship between the various estimates of soil flux computed by `neonSoilFlux` and the field-measured fluxes within daily interval periods. Statistics for these comparisons are reported in Figure 6, which also shows how these fall relative to a 1:1 line.

4.2 Effects of method choice on diffusivity estimates

In four of six field sites, the *post hoc* D_a estimate fell roughly between the two diffusion estimation methods; however this was less the case in the two driest sites, SJER and SRER (Table 1), where the field estimate of diffusivity was either lower or higher than both of the other methods (Figure 7).

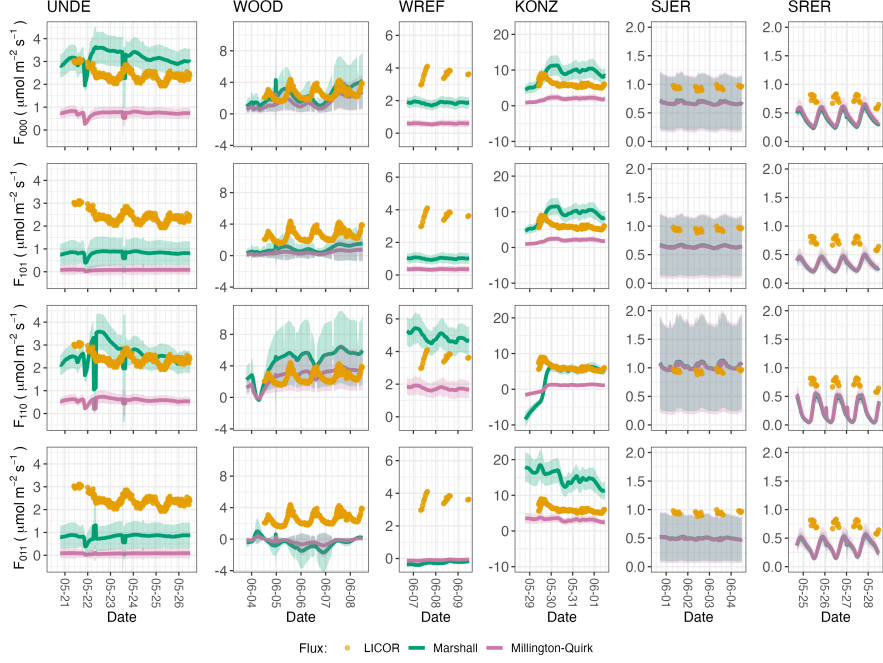


Figure 4: Timeseries of soil surface flux (F_S) from field-measured (yellow lines) and modeled soil fluxes (green or purple lines) by the `neonSoilFlux` R package. Fluxes from the `neonSoilFlux` R package are separated by the diffusivity model used (Millington-Quirk or Marshall, Section 3.2.2). Individual vertical axis labels in the first column represent the measurement levels where the flux-gradient approach is applied (Section 3.2.3). Ribbons for modeled soil fluxes represent ± 1 standard deviation. Results are reported in local time. WREF, SJER, and SRER were sampled in 2022, and UNDE, WOOD, and KONZ were sampled in 2024. Sites (columns) are arranged from left to right in terms of increasing mean annual temperature.

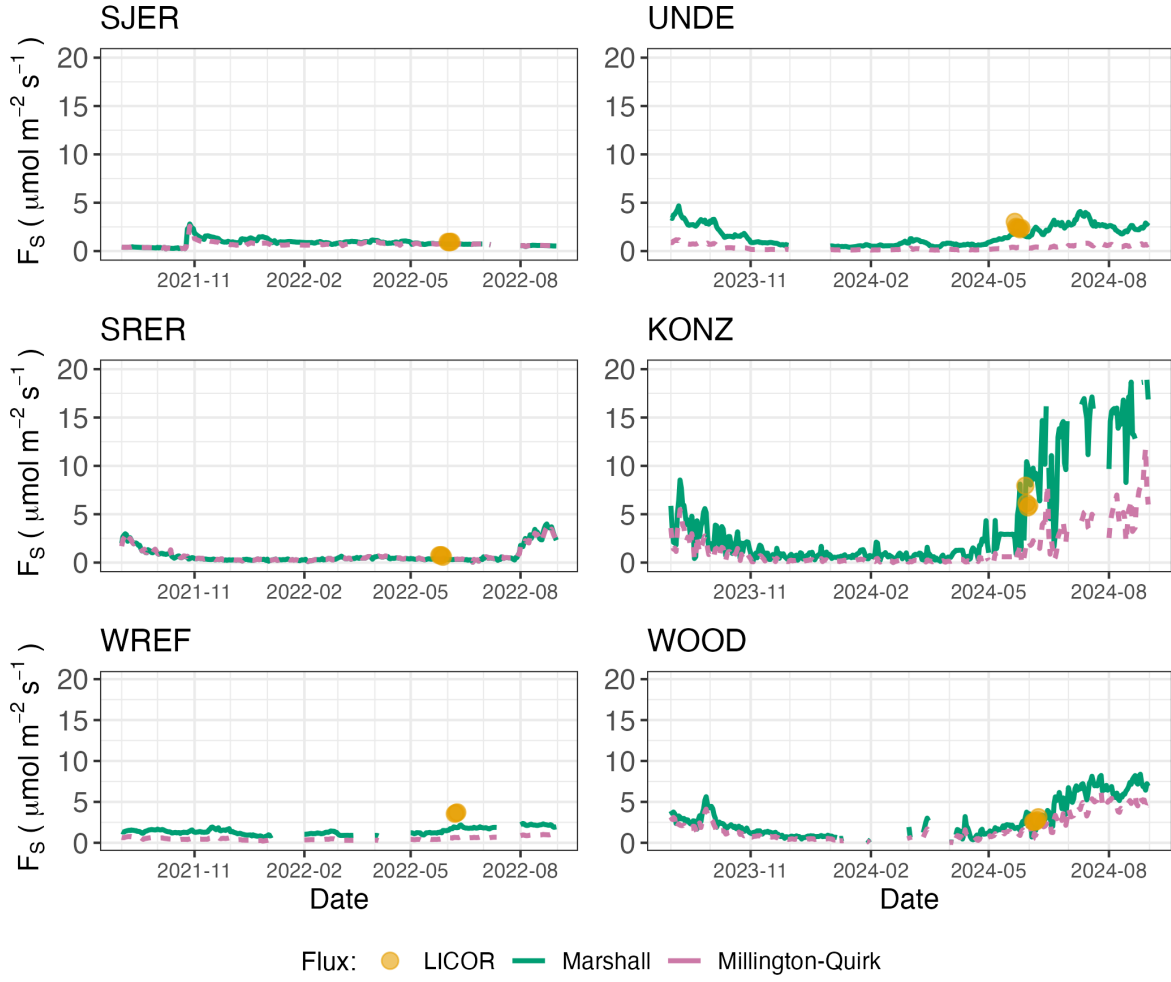


Figure 5: Timeseries of both daily-averaged field F_S (yellow circles) and daily ensemble averaged soil fluxes (average of F_{000} , F_{101} , F_{011} , F_{110} , Section 3.2.3) by the `neonSoilFlux` R package, separated by the diffusivity model used (green or purple lines, Millington-Quirk or Marshall, Section 3.2.2).

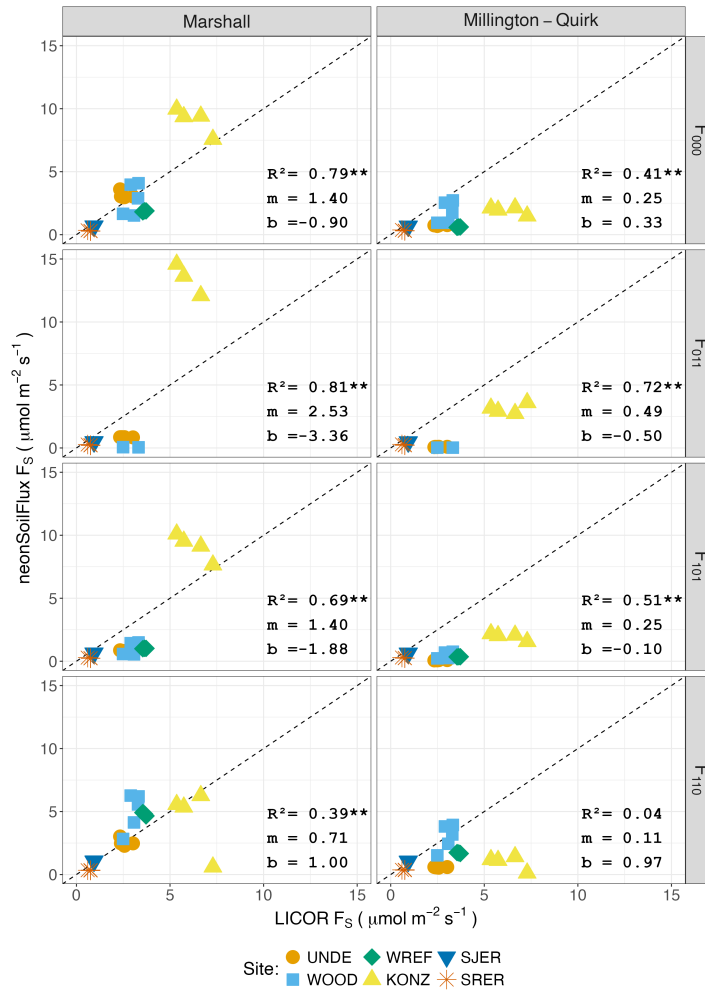


Figure 6: Statistical comparison between measured fluxes at each NEON site with fluxes reported by `neonSoilFlux` with the different flux calculation approaches and diffusivity calculations applied. Points are daily averages and LICOR F_S values are from the 6800 instrument only, for consistency. The dotted line represents a 1:1 relationship, and the reported R^2 quantifies the relationship between field-measured and `neonSoilFlux` estimated fluxes. * = significance at the 5% level, ** = significance at the 1% level. The slope (m) and intercept (b) of the linear regression between measured and modeled fluxes are also reported. The low-value outlier from KONZ in the F_{110} Marshall plot is an example of the effect of inverted CO₂ gradients causing an estimated flux to be negative, bringing down the daily mean, which later resolved as the soils dried back out.

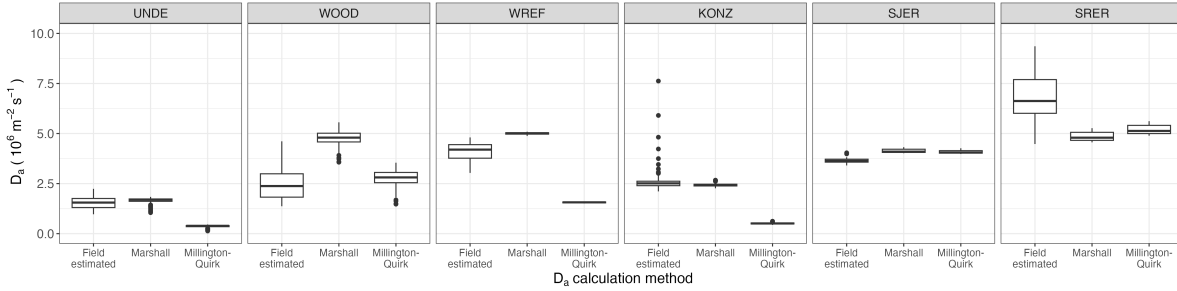


Figure 7: Distribution of diffusivity (D_a) at each study site. Values of D_a were provided by the `neonSoilFlux` package, computed from the Millington-Quirk or Marshall models (Section 3.2.2). A post-hoc estimate of diffusivity (labeled as “Field estimated”) was computed through the field measured flux (Figure 4), divided by the CO_2 gradient from the measurement levels closest to the soil surface, as reported by NEON. We only used F_S measured by the LICOR 6800 at all sites to standardize comparisons.

5 Discussion

This study presents a unified data science workflow to efficiently process automated measurements of belowground soil CO_2 concentrations, soil water content, and soil temperature to infer estimates of soil surface CO_2 effluxes through application of Fick’s Law (Equation 4). Our core goals in this study were: (1) to generate estimates of soil flux from continuous soil sensor data at terrestrial NEON sites using the flux-gradient method and then (2) to compare those estimates to field-measured fluxes based on the closed chamber approach at six NEON focal sites. We discuss our progress toward these core goals through (1) an overall evaluation of the flux-gradient approach (and uncertainty calculation) and (2) site-specific evaluation of differences in estimated vs measured fluxes.

5.1 General evaluation of flux-gradient approach

Key assumptions of the flux-gradient approach are that CO_2 concentrations increase throughout the soil profile such that the highest concentrations are observed in the deepest layers. Ad-

ditionally, field flux measurements should correlate with F_{000} because they represent surface fluxes. Periods where this gradient condition are not met generally are connected to processes that occur during soil wetting events, where more shallow soil layers produce higher concentrations of CO₂ due to microbial respiration pulses following rewetting. This effect is likely to be largest at sites with rich organic soils (e.g. KONZ). Based on this reasoning, in these types of situations we would *a priori* expect F_{011} (deepest layers) $\leq F_{101} \leq F_{110}$ (shallow layers) $\leq F_{000}$ (all layers) because the previous flux estimates rely primarily on CO₂ concentrations at deeper depths, and could miss high concentrations of CO₂ produced in shallower layers.

When modeling soil respiration, typically a non-linear response function that also considers soil type is used (Bouma & Bryla, 2000; Yan et al., 2016, 2018). For the `neonSoilFlux` package, soil type is connected to the measurement of bulk density, which was characterized at each NEON site. This bulk density estimate is based on replicate samples collected from the site megapit at a subset of soil horizons, with an estimated uncertainty of $\pm 5\%$ (NEON, 2024c). Coarse fragment estimates also have very large uncertainties, but because the volume fraction tends to be low in surface soils it is unlikely to contribute much additional flux uncertainty.

Our results suggest that the most important way to improve reliability of the flux estimate is to reduce the usage of gap-filled data. The current approach to gap filling in `neonSoilFlux` uses monthly mean data to gap fill—this approach decreases the ability of the estimate to be responsive to short-term pulses that occur with rapid weather shifts. Four sites (KONZ, SRER, WREF, and UNDE) had more than 75% of half-hourly periods with no-gap filled measurements (Figure S1, Supplementary Information). Two sites (SJER and WOOD) had more than 75% of half-hourly intervals with just one gap-filled measurement. The large uncertainty evident in Figure 4 for estimates from WOOD and SJER are thus due in part to the gap-filling used in these sites (Figure S1). While we did not need to use gap-filled measurements to compute the flux at WREF, field data collection occurred following a severe rainstorm, with soils at the

beginning of the sampling week near their water holding capacity. In general, we recommend that whenever possible, knowledge of local field conditions should influence analysis decisions in addition to any QA filtering protocols in the `neonSoilFlux` package.

We recognize that this gap-filling approach may lead to gap-filled values that are quite different from the actual values, such as an underestimate of soil moisture following rain events. Further extensions of the gap filling method could use more sophisticated gap-filling routines, similar to what is used for net ecosystem carbon exchange (Falge et al., 2001; Liu et al., 2023; Mariethoz et al., 2015; Moffat et al., 2007; Zhang et al., 2023). Additionally, since the deepest temperature and soil moisture sensors are located below the deepest CO₂ sensors at NEON sites, it is possible that excluding these deeper layers from consideration prior to analysis would lead to a reduced need for gap filling. Future iterations of the `neonSoilFlux` package may incorporate this as an option. The current gap-filling routine provides a consistent approach that can be applied to each data stream, but further work may explore alternative gap-filling approaches.

5.2 Evaluation of flux-gradient approach at each site

Derived results from the `neonSoilFlux` package have patterns that are broadly consistent with those directly measured in the field (Figure 4 and Figure 5), even though statistical comparisons between the field-measured and `neonSoilFlux` values were quite variable (e.g. R^2 ranging from 0.04 to 0.81; Figure 6). One advantage of the `neonSoilFlux` package is its ability to calculate fluxes across different soil depths (Figure 3), which allows for additional site-specific customization. We believe the package can provide a useful baseline estimate of soil fluxes that can always be complemented through additional field measurements.

The six locations studied provide a range of case studies that suggest different considerations may apply to different sites when applying the flux-gradient method. For example, the Santa

384 Rita Experimental Range (SRER) is a desert site characterized by sandy soil, which also was
385 the location of the highest field soil temperatures that we observed (Table 2). At SRER the
386 flux across the top two layers (F_{110}) produced a pattern of soil flux most consistent with the
387 observed field data. The remaining methods F_{101} , F_{011} , or F_{000} are derived from information
388 taken from the deepest layer, which seems to have been decoupled from the surface layers both
389 in terms of temperature and CO₂ concentration. This may be a general circumstance where
390 there are large diurnal temperature extremes that rapidly change during the course of a day
391 and overnight, leading to lags in the timing of when temperature increases propagate down to
392 deeper soil layers.

393 Immediately prior to our visit to Konza Prairie (KONZ), that site that experienced a significant
394 rain event that led to wet soils that gradually dried out over the course of our time there.
395 This pulse of precipitation increased the soil CO₂ concentration at the top layer above the
396 concentrations in lower layers, leading to negative estimated flux values at the start of the
397 field sampling period. In this case it was only when the soil began to return to a baseline level
398 that the assumptions of the flux-gradient method were again met.

399 Both of the previous cases also provide context for the variable statistical comparisons between
400 field-measured soil fluxes and `neonSoilFlux` outputs (Figure 6). When considering systematic
401 deployment of this method across a measurement network, there are a number of independent
402 challenges that require careful consideration. There are clear tradeoffs between (1) accuracy
403 of modeled fluxes (defined here as closeness to field-measured F_S and the uncertainty reduc-
404 tion factor ϵ), (2) precision (which could be defined by the signal to noise ratio), and (3) the
405 choice of the diffusivity model (Section 3.2.2) or flux computation method (Section 3.2.3). A
406 sensitivity analysis (Figure S2, Supplemental Information) found that flux output uncertainty
407 was dominated by measurement uncertainty (T_S , P , SWC , or CO₂) rather than by the dif-
408 fusivity method used to compute soil flux. Notably, the F_{110} method was least sensitive to

409 measurement uncertainty likely because it best aligns with the surface chamber measurement
410 assumptions.

411 Finally, comparing the effects of different diffusivity estimation methods on the match between
412 modeled and measured fluxes (Figure 5) highlights the sensitivity of F_{ijk} to diffusivity. The
413 comparison between diffusivity estimates compared to field estimated diffusivity (Figure 7)
414 demonstrates that site parameters can dictate which measure of diffusivity is most likely to
415 be accurate in a given environmental context. Site-specific differences are largely a reflec-
416 tion of differences in soil moisture across the sites (Table 1), as not all diffusivity estimation
417 methods incorporate soil moisture equivalently. While we here have compares two approaches
418 to calculate diffusivity (the Millington-Quirk and Marshall models), it may be valuable to
419 evaluate other diffusivity models (e.g. the Moldrup model; Moldrup et al. (1999)) as well. Ul-
420 timately the choice of a particular diffusivity model could be determined based on knowledge
421 of site-specific evaluations or a set of these models could be used to generate a model ensemble
422 average as a means to trade precision for a more general approach.

423 5.3 Recommendations for future method development

424 The `neonSoilFlux` package provides several approaches to estimate soil flux using the gradient
425 method. We believe these approaches enable the software to be used across a range of site-
426 specific assumptions (Maier & Schack-Kirchner, 2014). We note, however, that this choice
427 can have a determinative approach on the calculated values. Ensemble averaging approaches
428 (Elshall et al., 2018; Raftery et al., 2005) may be one way to address this problem if the goal is
429 to calculate fluxes using the same method at a diverse range of different sites. Two other ideas
430 would be to apply machine learning algorithms (e.g. random forest) to generate a single flux
431 estimate across diverse sites, or using co-located estimates of net ecosystem carbon exchange

⁴³² from eddy-flux towers to further constrain results or to assess soil flux results for plausibility
⁴³³ (Phillips et al., 2017).

⁴³⁴ These challenges notwithstanding, the method used here and made available in the
⁴³⁵ `neonSoilFlux` R package has the potential to produce nearly continuous estimates of flux
⁴³⁶ across all terrestrial NEON sites. These estimates are a significant improvement on available
⁴³⁷ approaches to constrain the portion of ecosystem respiration attributable to the soil. This,
⁴³⁸ in turn, also aids in our ability to understand the soil contribution to the net ecosystem flux
⁴³⁹ measured at these sites using the co-located eddy flux towers.

⁴⁴⁰ **6 Conclusions**

⁴⁴¹ We used the R package `neonSoilFlux` to estimate soil CO₂ fluxes with the flux-gradient
⁴⁴² method using data from buried soil sensors at NEON terrestrial sites. We compared the
⁴⁴³ predicted fluxes to those measured directly using a field-based closed chamber approach. Soil
⁴⁴⁴ fluxes from `neonSoilFlux` were broadly effective at producing estimates of flux comparable
⁴⁴⁵ to those measured in the field using a chamber-based technique. However `neonSoilFlux`
⁴⁴⁶ outputs are quite sensitive to a number of issues, including: missing data (and thus gap-
⁴⁴⁷ filling of input measurement datasets), the selection of soil depths used to best calculate the
⁴⁴⁸ gradient (which may vary between sites), and finally the choice of method used for estimating
⁴⁴⁹ soil diffusivity. The flexibility of the `neonSoilFlux` package allows the user to evaluate each
⁴⁵⁰ of these issues with site-specific knowledge and contexts. Future refinements and subsequent
⁴⁵¹ validation of `neonSoilFlux` outputs will feed forward into evaluating soil carbon fluxes broader
⁴⁵² spatial scales to enhance understanding of the ways in which soils across diverse ecosystems
⁴⁵³ are responding to a changing climate.

454 **Sources Cited**

- 455 Ayres, E., Reichle, R. H., Colliander, A., Cosh, M. H., & Smith, L. (2024). Validation of
456 Remotely Sensed and Modeled Soil Moisture at Forested and Unforested NEON Sites.
457 *IEEE Journal of Selected Topics in Applied Earth Observations and Remote Sensing*, 17,
458 14248–14264. <https://doi.org/10.1109/JSTARS.2024.3430928>
- 459 Baldocchi, D. (2014). Measuring fluxes of trace gases and energy between ecosystems and the
460 atmosphere - the state and future of the eddy covariance method. *Global Change Biology*,
461 20(12), 3600–3609. <https://doi.org/10.1111/gcb.12649>
- 462 Berenbaum, M. R., Carpenter, S. R., Hampton, S. E., Running, S. W., & Stanzione, D. C.
463 (2015). *Report from the NSF BIO Advisory Committee Subcommittee on NEON Scope
464 Impacts*.
- 465 Bond-Lamberty, B. (2018). New Techniques and Data for Understanding the Global Soil Res-
piration Flux. *Earth's Future*, 6(9), 1176–1180. <https://doi.org/10.1029/2018EF000866>
- 466 Bond-Lamberty, B., Ballantyne, A., Berryman, E., Fluet-Chouinard, E., Jian, J., Morris, K.
467 A., Rey, A., & Vargas, R. (2024). Twenty Years of Progress, Challenges, and Opportuni-
468 ties in Measuring and Understanding Soil Respiration. *Journal of Geophysical Research:
469 Biogeosciences*, 129(2), e2023JG007637. <https://doi.org/10.1029/2023JG007637>
- 470 Bond-Lamberty, B., Christianson, D. S., Malhotra, A., Pennington, S. C., Sihi, D., AghaK-
471 ouchak, A., Anjileli, H., Altaf Arain, M., Armesto, J. J., Ashraf, S., Ataka, M., Baldocchi,
472 D., Andrew Black, T., Buchmann, N., Carbone, M. S., Chang, S.-C., Crill, P., Curtis, P.
473 S., Davidson, E. A., ... Zou, J. (2020). COSORE: A community database for continuous
474 soil respiration and other soil-atmosphere greenhouse gas flux data. *Global Change Biology*,
475 26(12), 7268–7283. <https://doi.org/10.1111/gcb.15353>
- 476 Bond-Lamberty, B., & Thomson, A. (2010). A global database of soil respiration data. *Bio-
477 geosciences*, 7(6), 1915–1926. <https://doi.org/10.5194/bg-7-1915-2010>

- 479 Bond-Lamberty, B., Wang, C., & Gower, S. T. (2004). A global relationship between the
480 heterotrophic and autotrophic components of soil respiration? *Global Change Biology*,
481 10(10), 1756–1766. <https://doi.org/10.1111/j.1365-2486.2004.00816.x>
- 482 Bouma, T. J., & Bryla, D. R. (2000). On the assessment of root and soil respiration for soils
483 of different textures: Interactions with soil moisture contents and soil CO₂ concentrations.
484 *Plant and Soil*, 227(1), 215–221. <https://doi.org/10.1023/A:1026502414977>
- 485 Chen, H., & Tian, H.-Q. (2005). Does a General Temperature-Dependent Q10 Model of Soil
486 Respiration Exist at Biome and Global Scale? *Journal of Integrative Plant Biology*, 47(11),
487 1288–1302. <https://doi.org/10.1111/j.1744-7909.2005.00211.x>
- 488 Davidson, E. A., Janssens, I. A., & Luo, Y. (2006). On the variability of respiration in
489 terrestrial ecosystems: Moving beyond Q10. *Global Change Biology*, 12, 154–164. <https://doi.org/10.1111/j.1365-2486.2005.01065.x>
- 490 Desai, A. R., Murphy, B. A., Wiesner, S., Thom, J., Butterworth, B. J., Koupaei-Abyazani, N.,
491 Muttaqin, A., Paleri, S., Talib, A., Turner, J., Mineau, J., Merrelli, A., Stoy, P., & Davis,
492 K. (2022). Drivers of Decadal Carbon Fluxes Across Temperate Ecosystems. *Journal of
493 Geophysical Research: Biogeosciences*, 127(12), e2022JG007014. <https://doi.org/10.1029/2022JG007014>
- 494
- 495 Efron, B., & Tibshirani, R. J. (1994). *An Introduction to the Bootstrap*. Chapman and
496 Hall/CRC. <https://doi.org/10.1201/9780429246593>
- 497 Elshall, A. S., Ye, M., Pei, Y., Zhang, F., Niu, G.-Y., & Barron-Gafford, G. A. (2018). Relative
498 model score: A scoring rule for evaluating ensemble simulations with application to micro-
499 bial soil respiration modeling. *Stochastic Environmental Research and Risk Assessment*,
500 32(10), 2809–2819. <https://doi.org/10.1007/s00477-018-1592-3>
- 501 Falge, E., Baldocchi, D., Olson, R., Anthoni, P., Aubinet, M., Bernhofer, C., Burba, G.,
502 Ceulemans, R., Clement, R., Dolman, H., Granier, A., Gross, P., Grünwald, T., Hollinger,
503 D., Jensen, N.-O., Katul, G., Keronen, P., Kowalski, A., Lai, C. T., ... Wofsy, S. (2001).

- 505 Gap filling strategies for defensible annual sums of net ecosystem exchange. *Agricultural*
506 and *Forest Meteorology*, 107(1), 43–69. [https://doi.org/10.1016/S0168-1923\(00\)00225-2](https://doi.org/10.1016/S0168-1923(00)00225-2)
- 507 Farrance, I., & Frenkel, R. (2012). *Uncertainty of Measurement: A Review of the Rules*
508 for *Calculating Uncertainty Components through Functional Relationships*. *The Clinical*
509 *Biochemist Reviews*, 33(2), 49–75.
- 510 Friedlingstein, P., O’Sullivan, M., Jones, M. W., Andrew, R. M., Hauck, J., Landschützer,
511 P., Le Quéré, C., Li, H., Luijkx, I. T., Olsen, A., Peters, G. P., Peters, W., Pongratz,
512 J., Schwingshackl, C., Sitch, S., Canadell, J. G., Ciais, P., Jackson, R. B., Alin, S. R., ...
513 Zeng, J. (2025). Global Carbon Budget 2024. *Earth System Science Data*, 17(3), 965–1039.
514 <https://doi.org/10.5194/essd-17-965-2025>
- 515 Hamdi, S., Moyano, F., Sall, S., Bernoux, M., & Chevallier, T. (2013). Synthesis analysis
516 of the temperature sensitivity of soil respiration from laboratory studies in relation to
517 incubation methods and soil conditions. *Soil Biology and Biochemistry*, 58, 115–126. <https://doi.org/10.1016/j.soilbio.2012.11.012>
- 519 Jackson, R. B., Lajtha, K., Crow, S. E., Hugelius, G., Kramer, M. G., & Piñeiro, G. (2017).
520 The Ecology of Soil Carbon: Pools, Vulnerabilities, and Biotic and Abiotic Controls.
521 *Annual Review of Ecology, Evolution and Systematics*, 48(Volume 48, 2017), 419–445.
522 <https://doi.org/10.1146/annurev-ecolsys-112414-054234>
- 523 Jian, J., Bailey, V., Dorheim, K., Konings, A. G., Hao, D., Shiklomanov, A. N., Snyder, A.,
524 Steele, M., Teramoto, M., Vargas, R., & Bond-Lamberty, B. (2022). Historically inconsis-
525 tent productivity and respiration fluxes in the global terrestrial carbon cycle. *Nature*
526 *Communications*, 13(1), 1733. <https://doi.org/10.1038/s41467-022-29391-5>
- 527 Jian, J., Vargas, R., Anderson-Teixeira, K., Stell, E., Herrmann, V., Horn, M., Kholod, N.,
528 Manzon, J., Marchesi, R., Paredes, D., & Bond-Lamberty, B. (2021). A restructured and
529 updated global soil respiration database (SRDB-V5). *Earth System Science Data*, 13(2),
530 255–267. <https://doi.org/10.5194/essd-13-255-2021>

- 531 Jiang, J., Feng, L., Hu, J., Liu, H., Zhu, C., Chen, B., & Chen, T. (2024). Global soil
532 respiration predictions with associated uncertainties from different spatio-temporal data
533 subsets. *Ecological Informatics*, 82, 102777. <https://doi.org/10.1016/j.ecoinf.2024.102777>
- 534 Jobbágy, E. G., & Jackson, R. B. (2000). The Vertical Distribution of Soil Organic Carbon
535 and its Relation to Climate and Vegetation. *Ecological Applications*, 10(2), 423–436. [https://doi.org/10.1890/1051-0761\(2000\)010%5B0423:TVDOSO%5D2.0.CO;2](https://doi.org/10.1890/1051-0761(2000)010%5B0423:TVDOSO%5D2.0.CO;2)
- 537 Jurasinski, G., Koebsch, F., Guenther, A., & Beetz, S. (2022). *Flux: Flux Rate Calculation
538 from Dynamic Closed Chamber Measurements*.
- 539 Liu, K., Li, X., Wang, S., & Zhang, H. (2023). A robust gap-filling approach for European
540 Space Agency Climate Change Initiative (ESA CCI) soil moisture integrating satellite
541 observations, model-driven knowledge, and spatiotemporal machine learning. *Hydrology
542 and Earth System Sciences*, 27(2), 577–598. <https://doi.org/10.5194/hess-27-577-2023>
- 543 Lunch, C., Laney, C., Mietkiewicz, N., Sokol, E., Cawley, K., & Network), N. (National. E. O.
544 (2025). *neonUtilities: Utilities for Working with NEON Data*.
- 545 Luo, Y., Ogle, K., Tucker, C., Fei, S., Gao, C., LaDeau, S., Clark, J. S., & Schimel, D. S. (2011).
546 Ecological forecasting and data assimilation in a data-rich era. *Ecological Applications*,
547 21(5), 1429–1442. <https://doi.org/10.1890/09-1275.1>
- 548 Maier, M., & Schack-Kirchner, H. (2014). Using the gradient method to determine soil gas
549 flux: A review. *Agricultural and Forest Meteorology*, 192–193, 78–95. <https://doi.org/10.1016/j.agrformet.2014.03.006>
- 550 Mariethoz, G., Linde, N., Jougnot, D., & Rezaee, H. (2015). Feature-preserving interpolation
551 and filtering of environmental time series. *Environmental Modelling & Software*, 72, 71–76.
553 <https://doi.org/10.1016/j.envsoft.2015.07.001>
- 554 Marshall, T. J. (1959). The Diffusion of Gases Through Porous Media. *Journal of Soil Science*,
555 10(1), 79–82. <https://doi.org/10.1111/j.1365-2389.1959.tb00667.x>
- 556 Millington, R. J., & Shearer, R. C. (1971). Diffusion in aggregated porous media. *Soil Science*,

- 557 111(6), 372–378.
- 558 Moffat, A. M., Papale, D., Reichstein, M., Hollinger, D. Y., Richardson, A. D., Barr, A. G.,
559 Beckstein, C., Braswell, B. H., Churkina, G., Desai, A. R., Falge, E., Gove, J. H., Heimann,
560 M., Hui, D., Jarvis, A. J., Kattge, J., Noormets, A., & Stauch, V. J. (2007). Comprehensive
561 comparison of gap-filling techniques for eddy covariance net carbon fluxes. *Agricultural and*
562 *Forest Meteorology*, 147(3), 209–232. <https://doi.org/10.1016/j.agrformet.2007.08.011>
- 563 Moldrup, P., Olesen, T., Yamaguchi, T., Schjønning, P., & Rolston, D. E. (1999). Modeling
564 diffusion and reaction in soils: 9. The Buckingham-Burdine-Campbell equation for gas
565 diffusivity in undisturbed soil. *Soil Science*, 164(2), 75.
- 566 NEON. (2024a). *Barometric pressure (DP1.00004.001)*. National Ecological Observatory
567 Network (NEON). <https://doi.org/10.48443/RT4V-KZ04>
- 568 NEON. (2024b). *Soil CO₂ concentration (DP1.00095.001)*. National Ecological Observatory
569 Network (NEON). <https://doi.org/10.48443/E7GR-6G94>
- 570 NEON. (2024c). *Soil physical and chemical properties, Megapit (DP1.00096.001)*. National
571 Ecological Observatory Network (NEON). <https://doi.org/10.48443/S6ND-Q840>
- 572 NEON. (2024d). *Soil temperature (DP1.00041.001)*. National Ecological Observatory Network
573 (NEON). <https://doi.org/10.48443/Q24X-PW21>
- 574 NEON. (2024e). *Soil water content and water salinity (DP1.00094.001)*. National Ecological
575 Observatory Network (NEON). <https://doi.org/10.48443/A8VY-Y813>
- 576 Norman, J. M., Kucharik, C. J., Gower, S. T., Baldocchi, D. D., Crill, P. M., Rayment, M.,
577 Savage, K., & Striegl, R. G. (1997). A comparison of six methods for measuring soil-
578 surface carbon dioxide fluxes. *Journal of Geophysical Research: Atmospheres*, 102(D24),
579 28771–28777. <https://doi.org/10.1029/97JD01440>
- 580 Pedersen, A. R. (2024). *HMR: Flux Estimation with Static Chamber Data*.
- 581 Phillips, C. L., Bond-Lamberty, B., Desai, A. R., Lavoie, M., Risk, D., Tang, J., Todd-Brown,
582 K., & Vargas, R. (2017). The value of soil respiration measurements for interpreting and

- 583 modeling terrestrial carbon cycling. *Plant and Soil*, 413(1), 1–25. <https://doi.org/10.1007/s11104-016-3084-x>
- 584
- 585 Raftery, A. E., Gneiting, T., Balabdaoui, F., & Polakowski, M. (2005). *Using Bayesian Model*
586 *Averaging to Calibrate Forecast Ensembles*. <https://doi.org/10.1175/MWR2906.1>
- 587 Rheault, K., Christiansen, J. R., & Larsen, K. S. (2024). goFlux: A user-friendly way to
588 calculate GHG fluxes yourself, regardless of user experience. *Journal of Open Source*
589 *Software*, 9(96), 6393. <https://doi.org/10.21105/joss.06393>
- 590 Sallam, A., Jury, W. A., & Letey, J. (1984). Measurement of Gas Diffusion Coefficient under
591 Relatively Low Air-filled Porosity. *Soil Science Society of America Journal*, 48(1), 3–6.
592 <https://doi.org/10.2136/sssaj1984.03615995004800010001x>
- 593 Shao, J., Zhou, X., Luo, Y., Li, B., Aurela, M., Billesbach, D., Blanken, P. D., Bracho, R.,
594 Chen, J., Fischer, M., Fu, Y., Gu, L., Han, S., He, Y., Kolb, T., Li, Y., Nagy, Z., Niu, S.,
595 Oechel, W. C., ... Zhang, J. (2015). Biotic and climatic controls on interannual variability
596 in carbon fluxes across terrestrial ecosystems. *Agricultural and Forest Meteorology*, 205,
597 11–22. <https://doi.org/10.1016/j.agrformet.2015.02.007>
- 598 Shao, P., Zeng, X., Moore, D. J. P., & Zeng, X. (2013). Soil microbial respiration from
599 observations and Earth System Models. *Environmental Research Letters*, 8(3), 034034.
600 <https://doi.org/10.1088/1748-9326/8/3/034034>
- 601 Sihi, D., Gerber, S., Inglett, P. W., & Inglett, K. S. (2016). Comparing models of microbial–
602 substrate interactions and their response to warming. *Biogeosciences*, 13(6), 1733–1752.
603 <https://doi.org/10.5194/bg-13-1733-2016>
- 604 Tang, J., Baldocchi, D. D., Qi, Y., & Xu, L. (2003). Assessing soil CO₂ efflux using continuous
605 measurements of CO₂ profiles in soils with small solid-state sensors. *Agricultural and Forest*
606 *Meteorology*, 118(3), 207–220. [https://doi.org/10.1016/S0168-1923\(03\)00112-6](https://doi.org/10.1016/S0168-1923(03)00112-6)
- 607 Tang, J., Misson, L., Gershenson, A., Cheng, W., & Goldstein, A. H. (2005). Continuous
608 measurements of soil respiration with and without roots in a ponderosa pine plantation

- 609 in the Sierra Nevada Mountains. *Agricultural and Forest Meteorology*, 132(3), 212–227.
610 <https://doi.org/10.1016/j.agrformet.2005.07.011>
- 611 Taylor, J. R. (2022). *An Introduction to Error Analysis: The Study of Uncertainties in Physical*
612 *Measurements, Third Edition* (3rd ed.). University Science Press.
- 613 Wilson, S. J., Bond-Lamberty, B., Noyce, G., Bittencourt Peixoto, R., & Megonigal, J. P.
614 (2024). Fluxfinder: An R Package for Reproducible Calculation and Initial Processing of
615 Greenhouse Gas Fluxes From Static Chamber Measurements. *Journal of Geophysical Re-*
616 *search: Biogeosciences*, 129(11), e2024JG008208. <https://doi.org/10.1029/2024JG008208>
- 617 Yan, Z., Bond-Lamberty, B., Todd-Brown, K. E., Bailey, V. L., Li, S., Liu, C., & Liu, C. (2018).
618 A moisture function of soil heterotrophic respiration that incorporates microscale processes.
619 *Nature Communications*, 9(1), 2562. <https://doi.org/10.1038/s41467-018-04971-6>
- 620 Yan, Z., Liu, C., Todd-Brown, K. E., Liu, Y., Bond-Lamberty, B., & Bailey, V. L. (2016).
621 Pore-scale investigation on the response of heterotrophic respiration to moisture conditions
622 in heterogeneous soils. *Biogeochemistry*, 131(1), 121–134. <https://doi.org/10.1007/s10533-016-0270-0>
- 624 Zhang, R., Kim, S., Kim, H., Fang, B., Sharma, A., & Lakshmi, V. (2023). Temporal
625 Gap-Filling of 12-Hourly SMAP Soil Moisture Over the CONUS Using Water Balance
626 Budgeting. *Water Resources Research*, 59(12), e2023WR034457. <https://doi.org/10.1029/2023WR034457>
- 628 Zhao, J. (2019). FluxCalR: A R package for calculating CO₂ and CH₄ fluxes from static
629 chambers. *Journal of Open Source Software*, 4(43), 1751. <https://doi.org/10.21105/joss.01751>
- 631 Zobitz, J., Ayres, E., O'Rourke, K., Werbin, Z., Lee, L., Abdi, R., Mehmeti, D., & Xiong, L.
632 (2024). *neonSoilFlux: Compute Soil Carbon Fluxes for the National Ecological Observatory*
633 *Network Sites*.
- 634 Zobitz, J., & Zimmerman, N. (2025). *Supporting Code and Data for neonSoilFlux: An R*

635 *Package for Continuous Sensor-Based Estimation of Soil CO₂ Fluxes.* Zenodo. <https://doi.org/10.5281/zenodo.17516320>